DOI: 10.1002/zaac.201000091

Nickel(II) *N*-Benzyl-*N*-methyldithiocarbamato Complexes as Precursors for the Preparation of Graphite Oxidation Accelerators

Zdeněk Trávníček,*[a] Richard Pastorek,[a] Pavel Štarha,[a] Igor Popa,[a] and Václav Slovák[b]

Keywords: Nickel; Homogeneous catalysis; Dithiocarbamato ligands; Thermochemistry; Graphite oxidation accelerator

Abstract. The nickel(II) *N*-benzyl-*N*-methyldithiocarbamato (BzMedtc) complexes [Ni(BzMedtc)(PPh_3)Cl] (**1**), [Ni(BzMedtc)(PPh_3)Br] (**2**), [Ni(BzMedtc)(PPh_3)I] (**3**), and [Ni(BzMedtc)(PPh_3)(NCS)] (**4**) were synthesized using the reaction of [Ni(BzMedtc)$_2$] and [NiX_2(PPh_3)$_2$] (X = Cl, Br, I and NCS). Subsequently, complex **1** was used for the preparation of [Ni(BzMedtc)(PPh_3)$_2$]ClO_4 (**5**), [Ni(BzMedtc)(PPh_3)$_2$]BPh_4 (**6**), and [Ni(BzMedtc)(PPh_3)$_2$]PF_6 (**7**). The obtained complexes **1**–**7** were characterized by elemental analysis, thermal analysis and spectroscopic methods (IR, UV/Vis, $^{31}P\{^1H\}$ NMR). The results of the magnetochemical and molar conductivity measurements proved the complexes as diamagnetic non-electrolytes (**1**–**4**) or 1:1 electrolytes (**5**–**7**). The molecular structures of **4** and **5**·H_2O were determined by a single-crystal X-ray analysis. In all cases, the Ni^{II} atom is tetracoordinated in a distorted square-planar arrangement with the S_2PX, and S_2P_2 donor set, respectively. The catalytic influence of selected complexes **1**, **3**, **5**, and **6** on graphite oxidation was studied. The results clearly indicated that the presence of the products of thermal degradation processes of the mentioned complexes has impact on the course of graphite oxidation. A decrease in the oxidation start temperatures by about 60–100 °C was observed in the cases of all the tested complexes in comparison with pure graphite.

Introduction

Many compounds with the dithiocarbamate (dtc) moiety have been reported up to now in connection with their applications. These compounds were found to be useful as fungicides [1] or accelerators of vulcanization [2]. However, the spectrum of potential use of these compounds may be also broadened on the field of in vitro anticancer activity as can be demonstrated by the following examples. The 4(*3H*)-quinazolinone derivatives with dithiocarbamate side chains, such as (3,4-dihydro-2-methyl-4-oxoquinazolin-6-yl)-methyl-[4-(4-fluorophenyl)piperazine]-1-carbodithioate, showed promising in vitro anticancer activity (IC_{50} = 0.5 μM) against human myelogenous leukaemia cell line (K562) [3]. Another dithiocarbamate derivative, 4-methylsulfinyl-1-(*S*-methyldithiocarbamyl)-butane (sulforamate), serves as a bearer of cancer chemopreventive effect [4]. The efficient protection of *N*-benzyl-D-glucamine-dithiocarbamate against cisplatin-induced nephrotoxicity (it is able to chelate platinum and thus to decrease the possibility of its reactions with sulfur-containing renal proteins or enzymes) has also been reported recently [5].

* Prof. Dr. Z. Trávníček
Fax: +420585 634 357
E-Mail: zdenek.travnicek@upol.cz
[a] Department of Inorganic Chemistry
Faculty of Science, Palacký University
Tř. 17. listopadu 12
77146 Olomouc, Czech Republic
[b] Department of Chemistry
Faculty of Science, University of Ostrava
30. dubna 22
701 03 Ostrava, Czech Republic

Several thousand transition metal complexes with the dithiocarbamate moiety have been prepared and reported to date and some of them are very promising from the biological activity point of view. The Pt^{II} complex of the [Pt(esdt)(py)Cl] composition (esdt = ethylsarcosinedithiocarbamate and py = pyridine) is highly cytotoxic against several human cancer cell lines, and moreover, this substance was not found as nephrotoxic, in contrast to cisplatin [6]. [Au(dmdt)X_2] and [Au(esdt)X_2] are the representatives of non-platinum complex with the promising anticancer activity, which is even higher than cisplatin (dmdt = *N*,*N*′-dimethyldithiocarbamate, X = Cl or Br) [7]. The antifungal activity, well-known for dithiocarbamate derivatives, was proved for tin(IV) complexes with pyrrolidine-dithiocarbamate [8].

Nickel is known as a suitable transition metal for the preparation of complexes and it is not surprising that over three thousand compounds (SciFinder, 2010) and 163 X-ray structures (Crystallographic Structural Database, CSD, version 5.30, September 2009 update) [9] involving an NiS_2CN motif have been reported to date. Among these compounds, the nickel(II) complexes involving the $NiPN(S_2CN)$ or $NiP_2(S_2CN)$ moiety, such as [Ni(4-MePzdtc)(PPh_3)(NCS)] [10], and [Ni(MeSdtc)(dppe)] [11], respectively, were described in literature [4-MePzdtc = 4-methylpiperazine-dithicarbamate anion, PPh_3 = triphenylphosphine, MeSdtc = *N*-methyl-*N*-sulfonyldithiocarbamate, dppe = 1,2-bis(diphenylphosphine)ethane]. However, no nickel complexes containing the *N*-benzyl-*N*-methyldithiocarbamate anion (BzMedtc) within the mentioned moieties have been reported to date.

The presented series of compounds follows a great number of nickel dithicarbamato complexes previously prepared at our

department [see 12, 13 and the references cited therein]. In this paper, we deal with seven nickel(II) complexes, whose structures, according to the literature research, for the first time involve a combination of the BzMedtc and PPh_3 ligands. The complexes $[Ni(BzMedtc)(PPh_3)X]$ (**1**–**4**) were synthesized from $[Ni(BzMedtc)_2]$, using its reaction with $[NiX_2(PPh_3)_2]$, where *X* stands for Cl^- (for the complex **1**), Br^- (**2**), I^- (**3**) and NCS^- (**4**). The $[Ni(BzMedtc)(PPh_3)_2]Y$ complexes ($Y = ClO_4^-$ for **5**, BPh_4^- for **6** and PF_6^- for **7**) were prepared by the reaction of complex **1** with the appropriate alkaline salt and triphenylphosphane (see Scheme 1). The products were characterized by various physical methods including $^{31}P\{^1H\}$ NMR spectroscopy. The X-ray structures of the representatives of both types of complexes, i.e. [Ni(BzMedtc)(PPh_3)(NCS)] (**4**) and $[Ni(BzMedtc)(PPh_3)_2]ClO_4 \cdot H_2O$ (**5**·H_2O), were determined by single-crystal X-ray analysis. The arrangement of these compounds is square-planar with the NiS_2PN (**4**) and NiS_2P_2 (**5**·H_2O) donor sets.

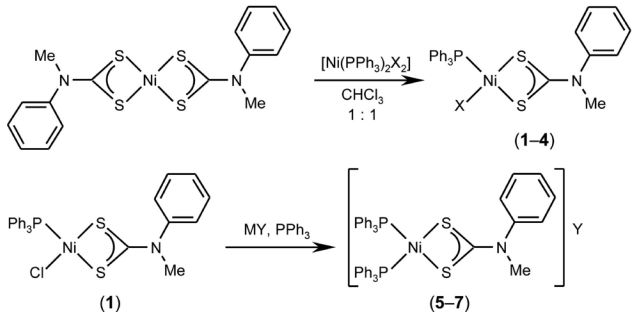

Scheme 1. Schematic representation of the synthetic procedures applied for the preparation of the nickel(II) complexes **1**–**7**; $X = Cl^-$ (**1**), Br^- (**2**), I^- (**3**) and NCS^- (**4**), $MY = LiClO_4 \cdot 3H_2O$ (**5**), $Na[BPh_4]$ (**6**) and $K[PF_6]$ (**7**).

This work also describes the effect of the nickel(II) dithiocarbamates on the oxidation of graphite as a model study of the coal combustion. As it is commonly known, the ignition temperature of the coal combustion is one of the most important properties influencing many industrial processes. This stage can be affected by the presence of both natural and artificial impurities [14, 15]. Formerly, several papers reported simple nickel(II) compounds, such as NiO (mixed with KOH) or $Ni(NO_3)_2$ (mixed with K_2SO_4), as the substances accelerating graphite oxidation [16, 17]. Few years ago, we decided to study the influence of the nickel(II, IV) dithiocarbamato complexes [see 13, 18, 19, and references cited therein] on the course of graphite oxidation. It was found that the presence of these complexes causes the ignition temperature decrease. Similar results were obtained also for the tested complexes **1**, **3**, **5**, and **6**, which were chosen as representatives of the presented compounds, as it is discussed in more detail within the framework of this paper.

Results and Discussion

The nickel(II) complexes **1**–**7** were prepared according to the synthetic strategies depicted in Scheme 1. The obtained molar conductivity values (Table 1) indicate that complexes **1**–**4** dissolved in acetone behave as non-electrolytes [20], which indirectly proved the coordination of the Cl^- (**1**), Br^- (**2**), I^- (**3**), and NCS^- (**4**) anions to the Ni^{II} atom. On the other hand, the molar conductivity values of the remaining complexes proved the ionic nature (1:1 electrolyte type) in acetone (**5**) or DMF (**6**, **7**) solutions, which means that the ClO_4^- (**5**), BPh_4^- (**6**), and PF_6^- (**7**) anions are situated outside of the inner coordination sphere within the structure of the discussed complexes. The results of the room temperature magnetic measurements determined the prepared compounds to be diamagnetic, and thus, suggested on square-planar arrangements in the vicinity of the central atom.

Spectroscopic Characterization

The PPh_3 signals in the $^{31}P\{^1H\}$ NMR spectra of the $CDCl_3$ solutions of **1**–**7** were found in the range of 21.1–32.1 ppm (Table 1). These values differ significantly from that of –4.52 ppm determined for the free PPh_3 molecule, which is caused by electron density redistribution from phosphorus towards the Ni^{II} atom as a consequence of PPh_3 coordination. The spectrum of **7** contains a septuplet at –143.6 ppm assignable to the PF_6^- anion. It should be noted that the chemical shift values of the complexes **1**–**4** increased in the order [Ni(BzMedtc)(PPh_3)Cl] (**1**) < [Ni(BzMedtc)(PPh_3)(NCS)] (**4**) < [Ni(BzMedtc)(PPh_3)Br] (**2**) < [Ni(BzMedtc)(PPh_3)I] (**3**), which is in agreement with the results reported for the nickel(II) complexes with *N*-benzyl-*N*-butyldithiocarbamate [12].

The maxima observed in the IR spectra of the nickel(II) complexes **1**–**7** at 990–998 cm^{-1}, and 1510–1542 cm^{-1} (see Table 1) are typical for the ν(C···S), and ν(C···N) vibrations of the dithiocarbamate moiety, respectively [21, 22]. The peak of the ν(C···S) stretching vibration is not split, which supports the bidentate coordination of the BzMedtc anion. The peaks of the ν(C≡N) and ν(C–S) vibrations of the NCS^- anion were observed in the IR spectrum of **4**. The ionic nature of the perchlorate anion in the complex **5**, can be supported by two undivided peaks at 622 and 1088 cm^{-1} [23]. The same conclusion can be made for the complex **7**, whose IR spectrum contains the non-split peak at 836 cm^{-1} assignable to ν(PF_6^-), which again indicates its ionic nature [24].

Diffuse-reflectance electronic spectra of the prepared complexes **1**–**7** support the assumption of the square-planar arrangement in the vicinity of the central Ni^{II} atom. Absorption maxima at the 18400–20700 cm^{-1} region may be attributed to the $^1A_{1g} \rightarrow {}^1B_{1g}$ transition of the square-planar nickel(II) complexes [25, 26]. The next maxima, also assignable to the *dd* transitions, were found for the complexes **1** (25200 cm^{-1}) and **2** (25000 cm^{-1}). The maxima above 29000 cm^{-1} are probably connected with the intraligand charge-transfer transitions in the S_2CN moiety [27].

X-ray Structure of [Ni(BzMedtc)(PPh$_3$)(NCS)] (4) and [Ni(BzMedtc)(PPh$_3$)$_2$]ClO$_4$·H$_2$O (5·H$_2$O)

The X-ray structure of the title complexes **4** (Figure 1) and **5**·H_2O (Figure 2) was determined by a single-crystal X-ray

Zeitschrift für anorganische und allgemeine Chemie ZAAC Journal of Inorganic and General Chemistry

Table 1. Results of molar conductivity measurements, IR, UV/Vis, and $^{31}P\{H\}$ NMR spectroscopy of the complexes **1**–**7**.

	λ_M [a]	IR /cm^{-1} [b]			UV/Vis /cm^{-1} [c]	$^{31}P\{H\}$ NMR δ [d] /ppm
		ν(C···S)	ν(C···N)	other		
1	2.2	990m	1510m		19 200 25 200 29 000	21.1s
2	2.1	996m	1520m		18 900 25 000 29 000	24.8s
3	9.3	998m	1520m		18 400 31 400	31.6s
4	1.7	996m	1528m	840m ν(C–S) 2092s ν(C≡N)	20 400 29 000	22.8s
5	99.0	996w	1542m	622m $\nu_4(ClO_4^-)$ 1088s $\nu_3(ClO_4^-)$	19 900 31 000	32.0s
6	77.3	990m	1536s		20 700 30 900	32.1s
7	66.9	996m	1540m	836m $\nu_4(PF_6^-)$	19 800 29 300	32.0s, –143.6sp

a) $S \cdot cm^2 \cdot mol^{-1}$ (10^{-3} M acetone solutions for **1**–**5** and 5×10^{-4} M DMF solutions for **6** and **7**).b) KBr pellets (w = weak, m = middle, s = strong).c) Nujol technique.d) $CDCl_3$ solutions (s = singlet, sp = septuplet).

analysis. The crystal data and structure refinements are given in Table 2, whereas the selected bond lengths and angles are summarized in Table 3.

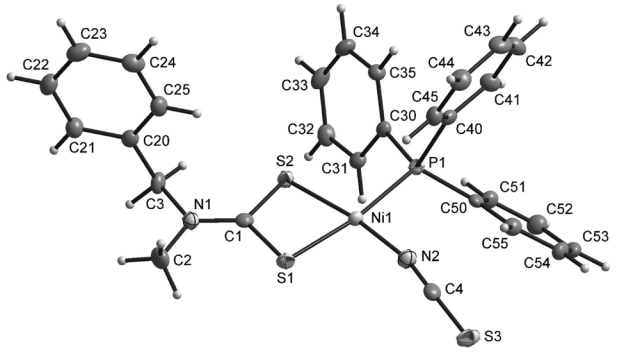

Figure 1. Molecular structure of [Ni(BzMedtc)(PPh_3)(NCS)] (**4**) with non-hydrogen atoms drawn as thermal ellipsoids at the 50 % probability level.

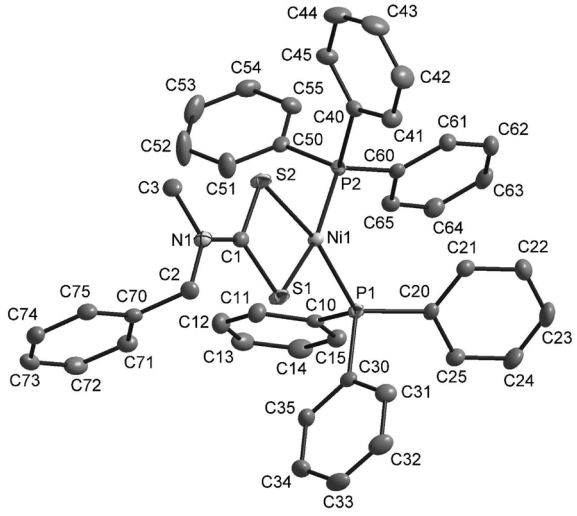

Figure 2. Molecular structure of [Ni(BzMedtc)(PPh_3)$_2$]$ClO_4 \cdot H_2O$ (**5**·H_2O) with non-hydrogen atoms drawn as thermal ellipsoids at the 50 % probability level. The hydrogen atoms, perchlorate anion, and water molecule of crystallization were omitted for clarity.

The central Ni^{II} atom of complex **4** (Figure 1) is tetracoordinated by PPh_3, the isothiocyanate anion, and the bidentate-coordinated *N*-benzyl-*N*-methyldithiocarbamate anion (BzMedtc). The atoms of a NiS_2NP chromophore are arranged in the distorted square-planar geometry around the metal center (Table 3). The Ni–S bond lengths of the title complex correlate well with the mean value of 2.204 Å (2.155–2.258 Å interval) determined for this band for the 116 square-planar nickel complexes involving bidentate-coordinated dithiocarbamato S-donor ligands, which have been up to now deposited in the Cambridge Structural Database (CSD) [9].

The well-known delocalization of π-electron density within the S_2CN moiety of the dithiocarbamate anion was observed for **4**, since the C–N and C–S bond lengths of the studied compound (Table 2) were found to be significantly shorter than the single C–N (1.47 Å) and C–S (1.81 Å) σ-bond lengths [28]. Further, the C–S and C–N bond length values of BzMedtc are comparable with those of the transition metal (TM) complexes involving the $(TM)S_2CNR_2$ moiety and deposited within the CSD, which equal 1.717 Å, and 1.326 Å, respectively.

The S1 atom is the most deviated one [0.0454(5) Å] from the plane created through the Ni1, S1, S2, P1, and N2 atoms of the chromophore. Further, the described plane forms the dihedral angle of 83.10(5)° with the benzene ring of the BzMedtc anion and dihedral angles of 67.90(5)°, 69.63(5)°, and 47.85(4)° with the benzene rings of PPh_3 containing the C30, C40, and C50 atoms, respectively. Mutual orientation of the phenyl groups of PPh_3 within the molecular structure of **4** can be described by the 67.64(6)° (between benzene rings containing C30 and C40), 66.06(6)° (between benzene rings containing C30 and C50) and 76.53(6)° (between benzene

Table 2. Crystal data and structure refinements for [Ni(BzMedtc)(PPh_3)(NCS)] (**4**) and [Ni(BzMedtc)(PPh_3)$_2$]ClO_4·H_2O (**5**·H_2O).

Compound	**4**	**5**·H_2O
Empirical formula	$C_{28}H_{25}N_2NiPS_3$	$C_{45}H_{42}ClNNiO_5P_2S_2$
Formula weight	575.36	897.02
Temperature /K	113(2)	110(2)
Wavelength /Å	0.71073	0.71073
Crystal system	Monoclinic	Triclinic
Space group	$P2_1/n$	$P\bar{1}$
a /Å	13.6177(3)	11.47995(13)
b /Å	10.3556(2)	13.24049(16)
c /Å	19.1287(4)	15.02884(19)
α /°	90	70.3319(11)
β /°	92.4015(18)	84.5683(10)
γ /°	90	87.3995(9)
V /Å^3	2695.6(9)	2141.23(4)
Z, D_{calc} /g·cm^{-3}	4, 1.418	2, 1.391
Absorption coefficient / mm^{-1}	1.032	0.734
Crystal size /mm	0.30 × 0.25 × 0.25	0.40 × 0.35 × 0.30
F (000)	1192	932
θ range for data collection /°	2.90 ≤ θ ≤ 25.00	3.03 ≤ θ ≤ 25.00
Index ranges (h, k, l)	–16 ≤ h ≤ 16 –9 ≤ k ≤ 12 –22 ≤ l ≤ 22	–13 ≤ h ≤ 13 –15 ≤ k ≤ 15 –17 ≤ l ≤ 15
Reflections collected/ unique (R_{int})	22656/4743 (0.0246)	18531/7526 (0.0108)
Max./min. transmission	0.7825/0.7471	0.8099/0.7578
Data/restraints/parameters	4743/0/317	7526/0/553
Goodness-of-fit on F^2	1.065	1.039
Final R indices [$I > 2\sigma(I)$]	R_1 = 0.0282, wR_2 = 0.0673	R_1 = 0.0342, wR_2 = 0.1009
R indices (all data)	R_1 = 0.0366, wR_2 = 0.0692	R_1 = 0.0388, wR_2 = 0.1031
Largest peak/hole /e·Å^{-3}	0.344/–0.212	1.343 and –0.611

Table 3. Selected bond lengths /Å and angles /° for the complexes [Ni(BzMedtc)(PPh_3)(NCS)] (**4**) and [Ni(BzMedtc) (PPh_3)$_2$]ClO_4·H_2O (**5**·H_2O).

Compound	**4**	**5**·H_2O
Bond lengths		
Ni1–S1	2.2245(5)	2.2154(6)
Ni1–S2	2.1758(5)	2.2257(6)
Ni1–P1	2.2162(5)	2.2165(6)
Ni1–P2	–	2.2316(6)
Ni1–N2	1.8564(17)	–
C1–S1	1.7125(19)	1.731(2)
C1–S2	1.7214(19)	1.721(2)
C1–N1	1.306(2)	1.307(3)
N2–C4	1.163(2)	–
C4–S3	1.621(2)	–
Bond angles		
S1–Ni1–S2	78.643(19)	78.29(2)
S1–Ni1–P1	171.63(2)	91.28(2)
S1–Ni1–N2	92.06(5)	–
S1–Ni1–P2	–	167.08(2)
S2–Ni1–P1	93.384(19)	167.76(2)
S2–Ni1–P2	–	88.91(2)
S2–Ni1–N2	170.70(5)	–
P1–Ni1–N2	95.91(5)	–
P1–Ni1–P2	–	101.24(2)
Ni1–S1–C1	85.71(7)	86.52(8)
Ni1–S2–C1	87.04(7)	86.42(8)
S1–C1–S2	108.60(11)	108.61(12)
S1–C1–N1	125.67(15)	126.50(17)
S2–C1–N1	125.73(15)	124.89(17)
Ni1–N2–C4	167.29(16)	–
N2–C4–S3	178.52(19)	–

rings containing C40 and C50) dihedral angles. The C–H···C, C–H···S and C···C types of the intermolecular non-bonding van der Waals contacts were detected to stabilize the crystal structure of **4** (see Table 4). No typical hydrogen bond is present within the structure of discussed complex.

In the case of **5**·H_2O, the Ni^{II} atom is tetracoordinated in the distorted square-planar arrangement (Figure 2), similarly to the above described structure of complex **4**, by the bidentate-coordinated S-donor BzMedtc ligand and by two P-donor PPh_3 molecules. Selected bond lengths and angles are given in Table 3. The positive charge of the [Ni(BzMedtc)(PPh_3)$_2$]$^+$ cation is compensated by the perchlorate anion; the shortest Ni1···Cl1 distance equals 7.131(2) Å.

As it has been already mentioned in the case of complex **4**, the bond lengths within the NiS_2CN moiety of both structures show on electron density redistribution in connection with π-electron density delocalization (see the C–S and C–N bond lengths in Table 3). As for the Ni–P bonds of **5**, their lengths are in good agreement with the mean value of 2.208 Å (2.175–2.252 Å interval) as determined from 36 X-ray structures of tetra-coordinated nickel dithiocarbamato complexes involving at least one PPh_3 ligand and deposited within the CSD.

The S2 atom is the most deviated one [0.0903(6) Å] from the plane created through the atoms of the chromophore. The dihedral angles between this plane and benzene rings involving C10, C20, C30, C40, C50, C60, and C70 are 86.39(5)°, 58.49(7)°, 87.97(5)°, 70.52(5)°, 71.64(5)°, 63.60(6)°, and 71.98(5)°, respectively. Non-bonding interactions of the C–H···C and C···C types (C–H···O interactions with the distorted perchlorate anion and water molecule of crystallization are disregarded) were found in the crystal structure of the discussed nickel(II) complex (Table 4).

TG/DTA Thermal Analysis

The thermal properties of the prepared nickel(II) complexes were studied by TG and DTA methods. The TG and DTA curves of **1** and **6** are depicted in Figure 3. Although the chemical composition of these complexes is different, their thermal decomposition proceeded in a similar manner as indicated by analogical shapes of the TG curves. In cases of **2**, **3** and **6**, the sharp *exo* effects with maxima at 188 °C, 193 °C, and 188 °C, respectively, were accompanied by mass increase on the TG curves, which can be attributed to the oxygen atom insertion into the Ni–P bond [29]. This effect was not registered on the TG curves of the remaining complexes, where the oxygen atom insertion is most likely combined with the decomposition of the organic parts of the studied complexes.

Zeitschrift für anorganische und allgemeine Chemie ZAAC Journal of Inorganic and General Chemistry

Table 4. Selected intermolecular non-bonding contacts and their parameters /Å,° determined for the complexes **4** and **5**·H_2O.

D–H···A	*d*(D–H)	*d*(H···A)	*d*(D···A)	<(DHA)
4				
C3–H3A···S3^{i}	0.990	2.9234(6)	3.666(2)	132.43(12)
C34–H34A···S2^{ii}	0.950	2.9389(5)	3.717(2)	139.90(12)
C32–H32A···S3^{iii}	0.950	2.8695(6)	3.814(2)	172.48(12)
C31–H31A···S1^{iii}	0.950	2.9701(6)	3.883(2)	161.56(12)
C2···C32			3.307(3)	
5·H_2O				
C74–H74A···C32^{iv}	0.950	2.771(3)	3.678(4)	160.13(16)
C72–H72A···C54^{v}	0.950	2.781(2)	3.554(3)	139.11(16)
C2–H2B···C74^{iv}	0.990	2.844(2)	3.771(3)	156.25(14)
C14–H14A···C33^{vi}	0.950	2.746(3)	3.666(4)	163.31(16)
C13–H13A···*C*3^{v}	0.950	2.879(2)	3.815(3)	168.16(14)
C44–H44A···C64^{vii}	0.950	2.872(3)	3.653(4)	140.17(16)
C13···C71^{v}			3.262(4)	
C70···C70^{iv}			3.391(3)	

Symmetry codes: (i) *x*+0.5, 0.5–*y*, *z*–0.5; (ii) 1–*x*, 1–*y*, 1–*z*; (iii) 1.5–*x*, *y*+0.5, 1.5–*z*; (iv) –*x*, –*y*, –*z*; (v) –*x*, 1–*y*, –*z*; (vi) 1–*x*, 1–*y*, –*z*; (vii) –*x*, 1–*y*, 1– *z*.

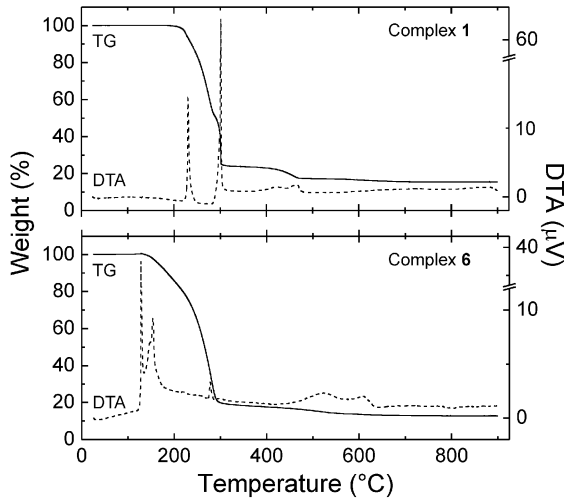

Figure 3. TG/DTA curves for complexes **1** and **6**.

The final products of the TG studies (900 °C) were studied by X-ray powder diffraction (XRD). NiO (PDF-4 No. 01-089-7130) was determined as final product of the thermal decomposition of **1**–**4**. In the cases of the complexes **6** and **7**, the mixtures with significant predominance of NiO were detected. The final product of the TG thermal study of **6** also contains NiS (PDF-4 No. 4-004-5027) and $Ni_3B_2O_6$ (PDF-4 No. 4-008-3203), and some peaks could not be assigned. As for the complex **7**, $Ni_2P_2O_7$ (PDF-4 No. 01-074-1604) and $Ni_3(PO_4)_2$ (PDF-4 No. 01-072-3977) were detected by an XRD, whereas some peaks were not assigned.

Catalytic Influence of the Complexes on Graphite Oxidation

The influences of the presence of complexes **1**, **3**, **5**, and **6** on graphite oxidation were studied. The results, summarized in Figure 4 (obtained DTG curves) and Table 5 (obtained data), showed a positive influence on graphite oxidation, because the ignition temperature significantly decreased (by about 64–99 °C) after the addition of the tested nickel(II) complexes to pure graphite.

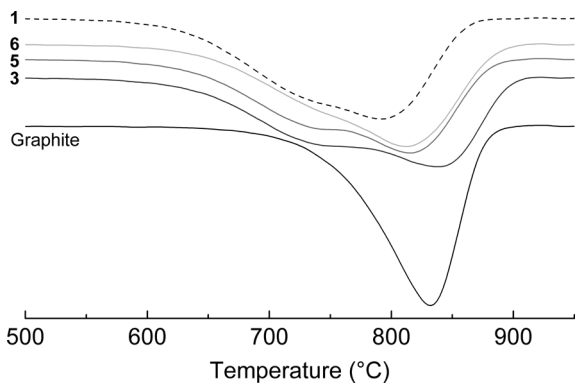

Figure 4. DTG curves obtained for pure graphite (black lines) and its mixture with the complexes **1** (black dashed lines), **3** (dark gray line), **5** (gray line), and **6** (light gray line); the tangent method was employed to determine the initial temperatures of the graphite oxidation.

Pure graphite oxidation proceeds in one step, whereas in the cases of its mixtures with the tested complexes, two steps in a larger temperature interval were detected on the appropriate DTG curves (Table 5). The first step takes place at lower temperature than pure graphite oxidation, whereas the oxidation rate maxima (T_m) of the second step approximately correspond to pure graphite. In addition, the oxidation mechanisms of both steps are different, as it can be seen from the activation energy (*E*) and frequency factor (*A*) values given in Table 5. More graphite was oxidized during the second step with higher *E* and *A* values.

At this point, we would like to discuss the described results of the influence on the graphite oxidation in connection with the results of TG/DTA studies. Figure 3 clearly shows that the thermal decomposition of the nickel(II) complexes is almost

Table 5. Characteristic temperatures and kinetic parameters of catalytic influence on graphite given for pure graphite and its mixtures with nickel(II) complexes **1**, **3**, **5** and **6**[a].

Sample	T /°C	T_m /°C	Step	n	A /s^{-1}	E	w /%
Graphite	778–859	832		0.7	1.97×10^9	247	
1	679–838	792	I	1.3	3.62×10^7	190	43.58
			II	0.9	1.09×10^9	235	56.42
3	696–879	838	I	0.9	4.08×10^6	174	34.48
			II	0.9	9.10×10^7	220	65.52
5	693–860	815	I	1.0	1.47×10^7	183	36.06
			II	1.0	4.08×10^9	250	63.94
6	714–861	812	I	0.	5.88×10^6	176	23.48
			II	1.1	1.17×10^9	238	76.52

a) T = temperature range of oxidation; T_m = oxidation rate maximum; n = reaction order; A = frequency factor; E = activation energy (kJ·mol^{-1}); w = mass of sample oxidized.

completely finished at the temperature of ca. 700 °C and the weight loss above this temperature is insignificant. Based on this statement it may be concluded that not directly the discussed nickel(II) *N*-benzyl-*N*-methyldithiocarbamato complexes, but the products of their thermal decomposition processes, affected graphite oxidation.

In connection with the above-mentioned facts, the tested complexes (except of **5**) were heated in situ to the temperatures corresponding to the beginning and end of graphite oxidation (see Table 5). The products of thermal decomposition relating to the mentioned temperatures were analyzed by XRD. As for **1**–**4**, pure NiO was identified at both temperatures (Figure 5). The slight differences in the 2θ values were caused by a dilatation of the sample due to different measurement temperature. On the other hand, the mixtures of NiO, NiS, and $Ni_3B_2O_6$ (for **6**) and $Ni_2P_2O_7$ and $Ni_3(PO_4)_2$ (for **7**) were detected by an XRD (Figure 5). Their quantitative composition was similar at both temperatures. Some peaks could not be assigned again.

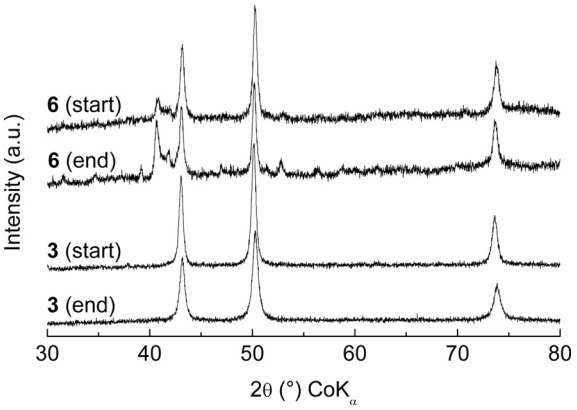

Figure 5. XRD patterns of the thermal decomposition products of the complexes **3** and **6**. The detected diffraction lines belong to NiO for **3**, and NiO, NiS, and $Ni_3B_2O_6$ for **6**; the start and end temperatures are given in Table 5.

Conclusions

Seven nickel(II) complexes of the [Ni(BzMedtc)(PPh_3)*X*] (**1**–**4**) and [Ni(BzMedtc)(PPh_3)$_2$]*Y* (**5**–**7**) compositions were synthesized (*X* = Cl^- for **1**, Br^- for **2**, I^- for **3** and NCS^- for **4**, *Y* = ClO_4^- for **5**, BPh_4^- for **6** and PF_6^- for **7**). The obtained powder products were fully characterized by elemental analysis, magnetic and molar conductivity measurements, thermal analysis and spectroscopic methods (IR, UV/Vis, $^{31}P\{^1H\}$-NMR). The molecular structures of the complexes [Ni(BzMedtc)(PPh_3)(NCS)] (**4**) and [Ni(BzMedtc)(PPh_3)$_2$]ClO_4·H_2O (**5**·H_2O) were determined by a single-crystal X-ray analysis, which proved the distorted square-planar arrangement with the bidentate-coordinated S-donor BzMedtc anion accompanied by PPh_3 and NCS^- (**4**) or by two PPh_3 (**5**). This paper also describes the significant catalytic influence of the thermal degradation products of the selected complexes **1**, **3**, **5**, and **6** on graphite oxidation.

Experimental Section

Materials and General Methods

Chemicals and solvents were purchased from Sigma–Aldrich Co., Acros Organics Co., Lachema Co. and Fluka Co. and they were used as received. The starting compounds [Ni(BzMedtc)$_2$], [Ni(PPh_3)$_2Cl_2$], [Ni(PPh_3)$_2Br_2$], [Ni(PPh_3)$_2I_2$], and [Ni(PPh_3)$_2$(NCS)$_2$] were prepared according to the formerly reported synthetic pathways [13, 30].

Elemental analyses (C, H, N) were performed with a Fisons EA-1108 CHNS-O Elemental Analyzer (Thermo Scientific). The content of nickel was determined using the chelatometric titration with murexide as an indicator. Chlorine, bromine, and iodine contents were determined with the Schöniger method. Diffuse-reflectance spectra were recorded with a Perkin–Elmer Lamda35 UV/Vis spectrometer using nujol techniques. IR spectra (KBr pellets) were recorded with a Perkin–Elmer Spectrum one FT-IR spectrometer in the 450–4000 cm^{-1} region. The molar conductivity values of 10^{-3} M acetone solutions of **1**–**5** and 5×10^{-4} M *N*,*N*'-dimethylformamide (DMF) solutions of **6** and **7** were determined with an LF 330/SET conductometer (WTW GmbH) at 25 °C. The room temperature magnetic susceptibilities were measured using the Faraday method with a laboratory designed instrument with a Sartorius 4434 MP-8 microbalance; Co[Hg(NCS)$_4$] was used as calibrant and the correction for diamagnetism was performed using Pascal constants.

Simultaneous thermogravimetric (TG) and differential thermal (DTA) analyses were performed with an Exstar TG/DTA 6200 (Seiko Instruments Inc.) in a platinum crucible and dynamic air atmosphere

(100 mL·min^{-1}) from the laboratory temperature to 950 °C with a 2.5 °C·min^{-1} temperature gradient. The weights of the studied complexes **1**–**4**, **6**, and **7** (**5** was not studied for safety reasons, since it contains the perchlorate anion) were ca. 10 mg. $^{31}P\{^1H\}$ NMR spectra of the $CDCl_3$ solutions were measured with a Bruker Avance 300 spectrometer at 300 K and the spectra were calibrated against 85 % H_3PO_4 used as an external reference. X-ray powder diffraction experiments were performed with a PANalytical X'Pert PRO instrument (Co-K_α radiation) equipped with an X'Celerator detector. Samples were placed on a zero-background silicon slide and scanned in the 2θ range of 5–90° in the steps of 0.017°. In situ measurements were realized in the reaction cell XRK900 (Anton Paar). Evaluation was made using HighScore Plus software and PDF-4 database.

Single Crystal X-ray Analysis of the Complexes 4 and 5·H_2O

Single-crystal X-ray measurements were performed with an Xcalibur^{TM}2 diffractometer (Oxford Diffraction Ltd.) with Sapphire2 CCD detector, and with Mo-K_α (Monochromator Enhance, Oxford Diffraction Ltd.) and at 113 K (**4**) and 110 K (**5**·H_2O). Data collection and reduction were performed by CrysAlis software [CrysAlis CCD and CrysAlis RED, Version 1.171.33.52, Oxford Diffraction Ltd., Abingdon, England, 2009]. The same software was used for data correction for an absorption effect by the empirical absorption correction using spherical harmonics, implemented in SCALE3 ABSPACK scaling algorithm. Both structures were solved by direct methods using SHELXS-97 software [31] and refined on F^2 using the full-matrix least-squares procedure (SHELXL-97). Non-hydrogen atoms were refined anisotropically and all hydrogen atoms were located in difference Fourier maps and refined by using the riding model with C–H = 0.95, 0.98, and 0.99 Å, and U_{iso}(H) = 1.2U_{eq}(CH, CH_2) or 1.5U_{eq}(CH_3), except for those belonging to the crystal water molecule in **5**. The perchlorate anion as well as crystal water molecule was refined as disordered over two positions with the occupancy factors 75 % and 25 %, and 57 % and 43 %, respectively. The crystal data and structure refinements of **4** and **5** are given in Table 1. The molecular graphics were drawn and the additional structural calculations were interpreted using DIAMOND [32].

Crystallographic data have been deposited with the Cambridge Crystallographic Data Centre, 12 Union Road, Cambridge CB21EZ, UK (Fax: +44-1223-336033; E-Mail: deposit@ccdc.cam.ac.uk). Copies of the data can be obtained free of charge on application to CCDC, as the depository numbers CCDC-766048 (**4**) and CCDC-766049 (**5**·H_2O).

Catalytic Studies

Graphite (0.6 g, diameter of particles less than 0.1 mm, ash residue max. 0.2 %, mass drying loss max. 0.2 %) was mixed with an acetone solution (2 mL) of the nickel(II) complex **1**, **3**, **5** or **6** (**2**, **4**, and **7** were not studied because of their insufficient solubility in acetone) to give the final nickel concentration of 2.5 mmol·L^{-1}. The mixtures were homogenized and dried at room temperature for 24 h. The study of the catalytic influence of these samples on graphite was performed with a Netzsch STA 449C device with an α-Al_2O_3 crucible without a standard (10 °C·min^{-1} heating rate, sample weight of 5.0 mg, 100 mL·min^{-1} dynamic air atmosphere). The intersection point of the DTG curve tangents represents the initial temperatures of the graphite oxidation. The kinetic parameters were calculated by a direct non-linear regression method [33].

Syntheses of the Nickel(II) Complexes 1–7

[Ni(BzMedtc)(PPh_3)Cl] (1), [Ni(BzMedtc)(PPh_3)Br] (2), [Ni(BzMedtc)(PPh_3)I] (3) and [Ni(BzMedtc)(PPh_3)(NCS)] (4): Complex **1** was synthesized using the reaction of [Ni(BzMedtc)$_2$] (1 mmol) and [$NiCl_2(PPh_3)_2$] (1 mmol). Both starting compounds were suspended in chloroform ($CHCl_3$) (each 25 mL). The mixture was stirred at room temperature until the reaction components were completely dissolved. The resulting solution was filtered through activated carbon. Diethyl ether was added to the filtrate, which was left to stand at laboratory temperature. The precipitate of **1** formed after a few days. The product was filtered off, washed with diethyl ether and dried at 40 °C under an infrared lamp. Complexes **2**–**4** were prepared as described for **1**, but [$NiBr_2(PPh_3)_2$] (for **2**), [$NiI_2(PPh_3)_2$] (for **3**) and [$Ni(NCS)_2(PPh_3)_2$] (for **4**) were used instead of [$NiCl_2(PPh_3)_2$]. In the case of the complex **4**, the crystals suitable for a single-crystal X-ray analysis were obtained from the mother liquor after two days.

[Ni(BzMedtc)(PPh_3)Cl] (1): Yield: 78 %. Color: violet. $C_{27}H_{25}NS_2PClNi$ (M_r = 552.8); C 58.7 (calcd. 58.4); H 4.6 (4.6); N 2.5 (2.4); S 11.6 (11.3); Cl 6.4 (6.5); Ni 10.6 (10.6) %. TG/DTA data: the decomposition began at 177 °C and was finished at 704 °C with the experimental weight loss of 84.5 % (calcd. to NiO residue: 86.5 %), exothermic peaks with the maxima at 231, 302, 420, and 463 °C.

[Ni(BzMedtc)(PPh_3)Br] (2): Yield: 90 %. Color: violet. $C_{27}H_{25}NS_2PBrNi$ (M_r = 597.2); C 54.3 (calcd. 54.2); H 4.2 (4.1); N 2.3 (2.0); S 10.7 (10.3); Br 13.4 (13.1); Ni 9.8 (9.6) %. TG/DTA data: the decomposition began at 156 °C and was finished at 1000 °C with the weight loss of 86.0 % (calcd. to NiO residue: 87.5 %), exothermic peaks with the maxima at 188, 282, 398, and 490 °C.

[Ni(BzMedtc)(PPh_3)I] (3): Yield: 70 %. Color: dark violet. $C_{27}H_{25}NS_2PINi$ (M_r = 644.2); C 50.3 (calcd. 49.9); H 3.9 (3.9); N 2.2 (2.2); S 10.0 (10.0); I 19.7 (19.3); Ni 9.1 (9.2) %. TG/DTA data: the decomposition began at 180 °C and was finished at 829 °C with the weight loss of 86.6 % (calcd. to NiO residue: 88.4 %), endothermic peak with the maximum at 269 °C and exothermic peaks with the maxima at 193, 246, 301, 457, and 544 °C.

[Ni(BzMedtc)(PPh_3)(NCS)] (4): Yield: 82 %. Color: red. $C_{28}H_{25}N_2S_3PNi$ (M_r = 575.4); C 58.5 (calcd. 58.9); H 4.4 (4.1); N 4.9 (4.7); S 16.7 (16.6); Ni 10.2 (10.3) %. TG/DTA data: the decomposition began at 155 °C and was finished at 1047 °C with the weight loss of 84.7 % (calcd. to NiO residue: 87.0 %), endothermic peak with the maximum at 198 °C and exothermic peaks with the maxima at 227, 304, 336, 442, and 541 °C.

[Ni(BzMedtc)(PPh_3)$_2$]ClO_4 (5): $LiClO_4$·3H_2O (2 mmol) was poured to a suspension of complex **1** (1 mmol) and PPh_3 (2 mmol) in methanol (25 mL). The reaction mixtures were heated under reflux for 3 h. The resulting solution was filtered through activated carbon and left to stand at room temperature. The crystals of **5**·H_2O suitable for a single-crystal X-ray analysis formed from the mother liquor after a few days. The complex was filtered off, washed with methanol and diethyl ether and dried at 40 °C under an infrared lamp. Yield: 47 %. Color: pink. $C_{45}H_{40}NS_2P_2ClO_4Ni$ (M_r = 879.0); C 61.5 (calcd. 61.8); H 4.6 (4.3); N 1.6 (1.5); S 7.3 (6.9); Cl 4.2 (4.6); Ni 6.7 (6.8) %.

[Ni(BzMedtc)(PPh_3)$_2$]BPh_4 (6): Na[BPh_4] (2 mmol) was added to a suspension of **1** (1 mmol) and PPh_3 (2 mmol) in methanol (25 mL). The reaction mixture was heated under for reflux 3 h during which a pink solid appeared. The product was removed by filtration, washed

(methanol and diethyl ether) and dried at 40 °C under an infrared lamp. Yield: 69 %. Color: pink. $C_{69}H_{60}NS_2P_2BNi$ (M_r = 1098.8); C 75.4 (calcd. 75.1); H 5.5 (5.2); N 1.3 (1.5); S 5.8 (5.6); Ni 5.3 (5.7) %. TG/DTA data: the decomposition began at 124 °C and was finished at 764 °C, exothermic peaks with the maxima at 128, 154, 178, 524, and 607 °C.

$[Ni(BzMedtc)(PPh_3)_2]PF_6$ (7): The solutions of PPh_3 (2 mmol; 5 mL of acetone) and $K[PF_6]$ (1 mmol; 7 mL of acetone) were separately added to a solution of **1** (1 mmol; 5 mL of chloroform). The reaction mixture was heated under refluxed for 4 h and afterwards filtered through activated carbon. Diethyl ether was added to the filtrate, which caused the formation of the precipitate. The solid was filtered off, washed with diethyl ether and dried at 40 °C under an infrared lamp. Yield: 54 %. Color: red. $C_{45}H_{40}NS_2P_3F_6Ni$ (M_r = 924.5); C 58.5 (calcd. 58.8); H 4.4 (4.6); N 1.6 (1.9); S 6.9 (6.5); Ni 6.3 (6.7) %. TG/DTA data: the decomposition began at 99 °C and was finished at 782 °C, exothermic peaks with the maxima at 188, 207, 310, and 472 °C.

Acknowledgement

This work was financially supported by the *Ministry of Education, Youth and Sports of the Czech Republic* (grant no. MSM6198959218). The authors also thank *Assoc. Prof. Zdeněk Šindelář* for magnetic susceptibility measurements, and *Dr. Jan Filip* for X-ray powder diffraction experiments.

References

[1] G. Hogarth, *Prog. Inorg. Chem.* **2005**, *53*, 71–561.
[2] P. J. Nieuwenhuizen, A. W. Ehlers, J. G. Haasnoot, S. R. Janse, J. Reedijk, E. J. Baerends, *J. Am. Chem. Soc.* **1999**, *121*, 163–168.
[3] S. L. Cao, Y. P. Feng, Y. Y. Jiang, S. Y. Liu, G. Y. Ding, R. T. Li, *Bioorg. Med. Chem.* **2005**, *13*, 1915–1917.
[4] C. Gerhauser, M. You, J. Liu, R. M. Moriarty, M. Hawthorne, R. G. Metha, R. C. Moon, J. M. Pezzuto, *Cancer Res.* **1997**, *57*, 272–278.
[5] S. Hidaka, T. Funakoshi, H. Shimada, M. Tsuruoka, S. Kojima, *J. Appl. Toxicol.* **1995**, *15*, 167–273.
[6] C. Marzano, F. Bettio, F. Baccichetti, A. Trevisan, L. Giovagnini, D. Fregona, *Chem. Biol. Interact.* **2004**, *148*, 37–48.
[7] L. Ronconi, C. Marzano, P. Zanello, M. Corsini, G. Miolo, C. Macca, A. Trevisan, D. Fregona, *J. Med. Chem.* **2006**, *49*, 1648–1657.
[8] D. C. Menezes, F. T. Vieira, G. M. de Lima, A. O. Porto, M. E. Cortés, J. D. Ardisson, T. E. Albrecht Schmitt, *Eur. J. Med. Chem.* **2005**, *40*, 1277–1282.
[9] F. A. Allen, *Acta Crystallogr., Sect. B: Struct. Sci.* **2002**, *58*, 380–388.
[10] B. Arul Prakasam, K. Ramalingam, R. Baskaran, G. Bocelli, A. Cantoni, *Polyhedron* **2007**, *26*, 1133–1138.
[11] M. R. L. Oliveira, J. Amim Jr., I. A. Soares, V. M. De Bellis, C. A. de Simone, C. Novais, S. Guilardi, *Polyhedron* **2008**, *27*, 727–733.
[12] R. Pastorek, J. Kameníček, J. Husárek, V. Slovák, M. Pavlíček, *J. Coord. Chem.* **2007**, *60*, 485–494.
[13] Z. Trávníček, R. Pastorek, V. Slovák, *Polyhedron* **2008**, *27*, 411–419.
[14] X. Gong, Z. Guo, Z. Wang, *Combust. Flame* **2010**, *157*, 351–356.
[15] Z. H. Wu, L. Xu, Z. Z. Wang, Z. R. Zhang, *Fuel* **2008**, *77*, 891–893.
[16] J. Carrazza, W. T. Tysoe, H. Heinemann, G. A. Somorjai, *J. Catal.* **1985**, *96*, 234–241.
[17] W. J. Lee, S. D. Kim, *Fuel* **1995**, *74*, 1387–1393.
[18] R. Pastorek, J. Kameníček, H. Vrbová, V. Slovák, M. Pavlíček, *J. Coord. Chem.* **2006**, *59*, 437–444.
[19] R. Pastorek, J. Kameníček, B. Cvek, V. Slovák, M. Pavlíček, *J. Coord. Chem.* **2006**, *59*, 911–919.
[20] W. J. Geary, *Coord. Chem. Rev.* **1971**, *7*, 81–122.
[21] C. A. Tsipis, D. P. Kessissoglou, G. A. Katsoulos, *Chim. Chron.,. New Ser.* **1985**, *14*, 195.
[22] S. V. Larionov, L. A. Patrina, I. M. Oglezneva, E. M. Uskov, *Koord. Chim.* **1984**, *10*, 92–99.
[23] R. P. Scholer, E. A. Merbach, *Inorg. Chim. Acta* **1975**, *15*, 15–20.
[24] L. Ballester, A. Gutierrez, M. F. Perpinan, C. Ruiz-Valero, *Polyhedron* **1996**, *15*, 1103–1112.
[25] A. B. P. Lever, in: *Inorganic Electronic Spectroscopy* (2nd ed.), Elsevier, Amsterdam, **1984**, p. 534.
[26] C. A. Tsipis, D. P. Kessissoglou, G. E. Manoussakis, *Inorg. Chim. Acta* **1982**, *65*, L137–L141.
[27] C. A. Tsipis, I. E. Meleziadis, D. P. Kessissoglou, G. A. Katsoulos, *Inorg. Chim. Acta* **1984**, *90*, L19–L22.
[28] *Handbook of Chemistry and Physics* (73rd ed.) (Ed.: D. R. Lide), CRC Press, Boca Raton, **1992**.
[29] F. Březina, E. Benátská, *J. Thermal. Anal.* **1981**, *22*, 75–79.
[30] *Gmelins Handbuch der Anorganischen Chemie*, Nickel, Teil C, Lief. 2, Verlag Chemie, GmbH, Weinheim, **1969**, p. 1043.
[31] G. M. Sheldrick, *Acta Crystallogr., Sect. A* **2008**, *64*, 112–122.
[32] K. Brandenburg, *DIAMOND, Release 3.1f*, Crystal Impact GbR, Bonn, Germany, **2006**.
[33] V. Slovák, *Thermochim. Acta* **2001**, *372*, 175–182.

Received: February 16, 2010
Published Online: May 7, 2010

